On the mechanisms of late 20th century sea-surface temperature trends over the Antarctic Circumpolar Current

Sergey Kravtsov,[1] Igor Kamenkovich,[2] Andrew M. Hogg,[3] and John M. Peters[1]

Received 26 July 2011; revised 2 September 2011; accepted 9 September 2011; published 23 November 2011.

[1] The Antarctic Circumpolar Current (ACC), with its associated three-dimensional circulation, plays an important role in global climate. This study concentrates on surface signatures of recent climate change in the ACC region and on mechanisms that control this change. Examination of climate model simulations shows that they match the observed late 20th century sea-surface temperature (SST) trends averaged over this region quite well, despite underestimating the observed surface-wind increases. Such wind increases, however, are expected to lead to significant cooling of the region, contradicting the observed SST trends. Motivated by recent theories of the ACC response to variable wind and radiative forcing, the authors used two idealized models to assess contributions of various dynamical processes to the SST evolution in the region. In particular, a high-resolution channel model of the ACC responds to increasing winds by net surface ACC warming due to enhanced mesoscale turbulence and associated heat transports in the mixed layer. These fluxes, modeled, in a highly idealized fashion, via increased lateral surface mixing in a coarse-resolution hybrid climate model, substantially offset zonally non-uniform surface cooling due to air-sea flux and Ekman-transport anomalies. These results suggest that the combination of these opposing effects must be accounted for when estimating climate response to any external forcing in the ACC region.

Citation: Kravtsov, S., I. Kamenkovich, A. M. Hogg, and J. M. Peters (2011), On the mechanisms of late 20th century sea-surface temperature trends over the Antarctic Circumpolar Current, *J. Geophys. Res.*, *116*, C11034, doi:10.1029/2011JC007473.

1. Introduction

[2] The Southern Ocean is a critical part of the global climate system, but lack of observational constraints and complexity of ocean currents there result in incomplete understanding of the Southern Ocean dynamics and substantial biases in climate model simulations of this region [*Russell et al.*, 2006; *Sloyan and Kamenkovich*, 2007]. One of the most intriguing features of the Southern Ocean is the Antarctic Circumpolar Current (ACC) [*Rintoul et al.*, 2001] whose structure and natural variability centrally involve the dynamics of mesoscale oceanic eddies [*Marshall and Radko*, 2003; *Hallberg and Gnanadesikan*, 2006; *Hogg and Blundell*, 2006; *Radko and Marshall*, 2006]. The orientation of ACC isopycnals, partly controlled by eddies, exerts a strong control on the global stratification [see, e.g., *Kamenkovich and Sarachik*, 2004; *Wolfe and Cessi*, 2010; *Radko and Kamenkovich*, 2011]. Yet, vast majority of climate models used for climate prediction in the region are still run at coarse resolutions and rely on parameterizations of mesoscale-eddy fluxes in terms of larger-scale variables to simulate ACC dynamics. These models, however, face a challenging task of capturing the response of complicated dynamics of ACC to variable atmospheric forcing.

[3] The ACC is driven by a combination of buoyancy and wind-forcing. Atmospheric observations indicate intensification of the polar vortex or, equivalently, a shift of the Southern Hemisphere Annular Mode (SAM) toward its high-index state over the second half of the 20th century [*Thompson et al.*, 2000; *Thompson and Solomon*, 2002; *Marshall*, 2003]. During the same period, the subsurface Southern Ocean warmed in the ACC region [*Gille*, 2002, 2008]. Climate model simulations that incorporate various anthropogenic and natural forcings capture both of these trends [*Fyfe*, 2006; *Fyfe and Saenko*, 2006], with quantitative details being sensitive to the particular subset of forcing factors considered. The major players affecting the SAM trend include greenhouse gas forcing [*Kushner et al.*, 2001; *Cai et al.*, 2005] combined with stratospheric ozone changes [*Gillett and Thompson*, 2003; *Shindell and Schmidt*, 2004; *Arblaster and Meehl*, 2006]. The relative importance of these factors is still under debate. *Marshall et al.* [2004] argued for the importance of natural forcings, while *Cai and Cowan* [2007] and *Cai et al.* [2006, 2010a] brought trends in anthropogenic aerosols into the dynamical picture

[1]Department of Mathematical Sciences, Atmospheric Sciences Group, University of Wisconsin-Milwaukee, Milwaukee, Wisconsin, USA.
[2]MPO, RSMAS, University of Miami, Miami, Florida, USA.
[3]Research School of Earth Sciences, Australian National University, Canberra, ACT, Australia.

0148-0227/11/2011JC007473

of recent SAM changes. This predominantly externally forced SAM trend contributes to the observed increase of the Southern Ocean heat content [*Oke and England*, 2004; *Cai et al.*, 2006, 2010b; *Fyfe et al.*, 2007], with possible coupled positive feedback on the SAM strength [*Marshall and Connolley*, 2006; *Cai and Cowan*, 2007].

[4] The response of ACC to changes in the atmospheric forcing is, however, complex and strongly affected by the eddy dynamics. In particular, *Meredith et al.* [2004] showed that despite considerable wind stress increase over ACC in the 80s and 90s, the ACC mass transport remained relatively constant during this period; instead, the response of the ocean to interannual or longer wind stress variations is to intensify oceanic mesoscale activity [*Meredith and Hogg*, 2006]. These results are consistent with later observational analyses of *Böning et al.* [2008] and with eddy-resolving three-dimensional simulations of the Southern Ocean by *Hallberg and Gnanadesikan* [2006]. *Hogg et al.* [2008] used an idealized eddy-resolving ACC model to demonstrate that enhanced horizontal mixing by eddies in response to increasing wind stress outweighs trends due to Ekman advection in the surface mixed layer, and suggested that eddy modifications play a similarly important role in the warming of the subsurface Southern Ocean. *Fyfe et al.* [2007] confirmed the latter assertion in simulations using an intermediate complexity climate model, in which the isopycnal eddy diffusivity linearly depended on the surface wind stress. *Shaffrey et al.* [2009] noted substantial quantitative differences in the Southern Ocean's heat transport between coarse-resolution and eddy-permitting versions of their global coupled model, while *Farneti and Delworth* [2010] and *Farneti et al.* [2010] were the first to simulate the compensating eddy effects on subsurface stratification in the climate-change experiments with an eddy-permitting global coupled climate model. These effects can be partially represented by modified eddy parameterization schemes in coarse-resolution climate models [*Gent and Danabasoglu*, 2011; *Farneti and Gent*, 2011].

[5] While earlier observational and modeling studies reviewed above focused primarily on the mesoscale eddy effects in the *subsurface* ocean, we here concentrate instead on eddy contributions to the *surface* signature of the climate change over the ACC region (compare with the recent observational study by *Sallée et al.* [2010]); hereafter, the ACC region is defined as the region between 60° and 40° S. In particular, we deploy idealized climate models in the spirit of *Fyfe et al.* [2007] and *Hogg et al.* [2008] studies to interpret the differences between the late 20th century surface climate change over the ACC detected in observations and in global climate model simulations performed within the Coupled Model Intercomparison Project phase 3 (CMIP3) [*Meehl et al.*, 2007]. These differences are outlined in section 2. Section 3 describes the set up and results from our idealized climate model simulations; we build upon these results to argue, among other things, that eddy-driven mixing at the surface is essential in the ACC-region surface-climate response to the external forcing. We summarize our results and further discuss their implications in section 4. The appendix enhances the model-data comparison of section 2 by processing an alternative observational data set using a different visualization technique, and by addressing the seasonal dependence of the model-data differences.

2. Observed and Simulated Surface Climate Trends Over the ACC

[6] We computed multimodel ensemble means of surface climate characteristics across the ensemble of CMIP3 20th century runs using the same model simulations as in *Kravtsov and Spannagle* [2008], and compared them with the corresponding observed time series. IPCC IDs of the models considered here are as follows: *CCCMA-CGCM*3.1, *CCSM*3, CNRM-CM3, CSIRO-MK3.0, *ECHAM5/MPI-OM*, ECHO-G, *GFDL-CM*2.0, *GFDL-CM*2.1, *GISS-AOM*, *GISS-EH*, *GISS-ER*, INM-CM3.0, IPSL-CM4, *MIROC*3.2*-medres*, *UKMO-HadCM*3, *UKMO-HadGEM*1; italicized acronyms above represent the models included in the 14-member ensemble analyzed by *Miller et al.* [2006], with the focus on forced trends in the annular modes.

2.1. Basin-Averaged Trends

[7] Figure 1a shows the model-data comparison for the sea-surface temperature (SST) anomalies (relative to the 1971–1999 climatology) averaged over the 40°–60° S latitudinal band corresponding to the ACC region; the observational analysis used ERSST data [*Smith et al.*, 2008]. The CMIP3 ensemble-mean SSTs closely follow the observed time series after about 1970, with interannual-to-decadal deviations that can easily be interpreted in terms of the observed natural climate variability. In particular, the observed SSTs appears to exhibit a sudden warming around the mid-1970s, concurrent with a major climate shift arguably related to intrinsic dynamics of the Earth climate system [*Graham*, 1994; *Tsonis et al.*, 2007], whereas the CMIP ensemble mean SSTs, which represent the forced signal, warm at a relatively uniform rate throughout the time period shown. The observations over the Southern Ocean prior to 1970s are, however, sparse and the basin-wide SST estimates derived from them are not reliable. Consequently, the model-data differences during this period are difficult to interpret. To avoid dealing with this issue and to make use of better data quality in the late 20th century [*Thompson and Solomon*, 2002; *Marshall*, 2003], we focus on the 1971–1999 period, during which the net CMIP3 simulated SST warming rate (Figure 1a, black line) is fairly consistent with the net observed rate (Figure 1a, dashed line).

[8] On the other hand, there are larger differences between the observed (ERA-40 [*Uppala et al.*, 2005]) and CMIP3 simulated sea level pressure (SLP) trends. Most importantly, the simulated trend is substantially weaker than the observed. These differences are visualized in Figure 1b by plotting zonal component of the geostrophic surface wind anomalies u_G area averaged over the 40°–60°S ACC region. The quantity u_G related to the meridional SLP gradient is, in fact, a very good approximation to the full zonal surface wind. The observed linear trend in u_G is of about 0.15 m s^{-1} per decade, or 3% per decade using climatological u_G value of 4.8 m s^{-1} derived from ERA-40 data, while the simulated ensemble-mean CMIP3 trend is several times smaller, at about 0.05 m s^{-1} per decade. The difference of 0.1 m s^{-1} per decade between the observed and simulated trends is statistically positive at 5% level according to the *t*-test for

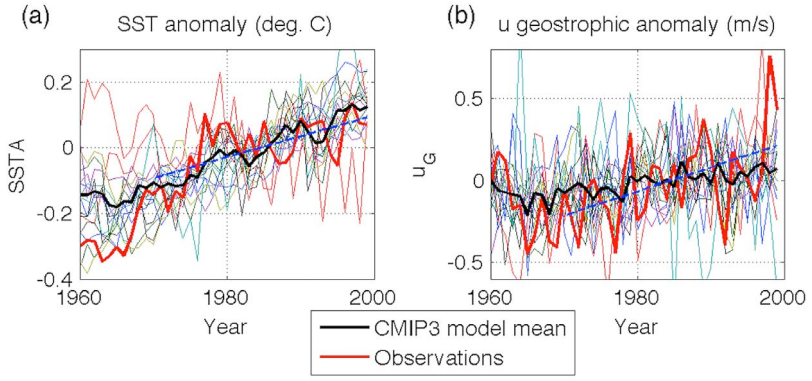

Figure 1. Observed and CMIP3 simulated annual-mean climate anomalies (relative to 1971–1999 climatology) in the ACC region (40°–60°S). (a) Sea-surface temperature (SST) and (b) zonal geostrophic wind u_G (observed climatological value (inferred from Figure 2): ~4.8 m s^{-1}). Thick red line, observations (ERSST for SST and ERA-40 for u_G); dashed blue line, 1971–1999 observed linear trend; thin colored lines, individual CMIP-3 models' ensemble means; thick black line, multimodel ensemble average.

trends applied to the 1971–1999 annual time series formed by differencing the observed and multimodel-mean u_G time series; in particular, the 5th percentile of the difference trend is positive and equal to 0.01 m s^{-1} per decade. To check for the sensitivity of this result to outliers, we also replaced the largest value of the observed u_G time series (which occurred at year 1998) with the second largest value (for year 1999) and repeated the test for the difference between observed and CMIP3-simulated trends. In that testing, the 5th percentile of the difference trend was very close to zero, thus indicating borderline significance of the trend difference. Note, however, that the results of the observed-versus-simulated trend comparison using the direct sea level pressure (rather than u_G) time series, as well as seasonal results provide an additional, and more striking evidence for the substantial differences between the evolution of the observed and simulated winds over the Southern Ocean in recent decades (see Appendix A).

[9] The causes of model-data differences in Figure 1b are numerous and possibly quite complex. Candidate reasons for the discrepancies include the lack of stratospheric ozone and/or natural, as well as anthropogenic aerosol forcing in many of the CMIP3 simulations considered here [*Marshall et al.*, 2004; *Miller et al.*, 2006; *Arblaster and Meehl*, 2006; *Cai et al.*, 2010a]. Furthermore, *Miller et al.* [2006] argue that the CMIP3 models underestimate the dynamical coupling of the forced stratospheric changes onto surface climate trends, including the surface winds.

[10] As a result of weaker SLP and surface velocity trends, the CMIP3 model ensemble underestimates, by a factor of 2–5, the observed increase of the wind stress over the ACC. The observed climatology and linear trend of the zonal wind stress are shown in Figure 2; the resulting estimate of fractional wind stress trend value over ACC region is of about 5–10% per decade. The latter fractional rate of change of wind stress exceeds that of wind speed since the wind stress is proportional to the square of the wind speed. We obtained analogous or even more striking results using alternative observational and seasonal-mean data sets (see Figures A1–A3). If the simulated wind stress forcing of the ocean is so different from observations, then why is the basin-averaged SST response so similar?

2.2. Trends in Two Dimensions

[11] We now turn to the CMIP3-model-data differences in terms of the two-dimensional SST trends over the Southern Ocean. Despite a fairly accurate simulation of the climatological SST (Figure 3) and the linear trend in area-averaged SST over the Southern Ocean (Figure 1a), the CMIP3 models exhibit significant biases in the spatial distribution of the linear SST trends (Figure 4). While there are some similarities in the spatial patterns of the observed (Figure 4b) and simulated (Figure 4a) SST trends (the pattern correlation between the observed and simulated linear SST trend fields is ~0.5), magnitudes of the trend are substantially different. In particular, the simulated SST trends at many individual locations throughout the Southern Ocean basin are substantially smaller than the observed ones.

[12] The pattern of zonally asymmetric SST trends is dictated by the zonal asymmetries in the Southern Ocean's wind trends (see, for example, Figure 2b), via a combination of the associated Ekman transports and air-sea heat flux anomalies [*Sallée et al.*, 2010]. The relative weakness of the zonal asymmetry in CMIP3 simulated SST trends documented in Figure 4 is likely to be associated with weaker-than-observed surface-wind intensification in CMIP3 models (see Figures 1b and A2). Note, once again, that despite the model-data differences in the patterns and magnitude of the SST trends in two dimensions (Figure 4), the *zonally averaged* observed and simulated SST trends (Figure 1a) are similar due to cancellations among the oppositely signed regional trends along the latitudinal circle.

2.3. Summary of Model-Data Comparison and Outstanding Questions

[13] In summary, the ensemble average of the CMIP3 20th century simulations is characterized by weaker-than-observed regional 1979–1999 SST trends over the ACC, but basin-averaged SST trends which are similar to the observed trends. The weaker regional SST trends are consistent with

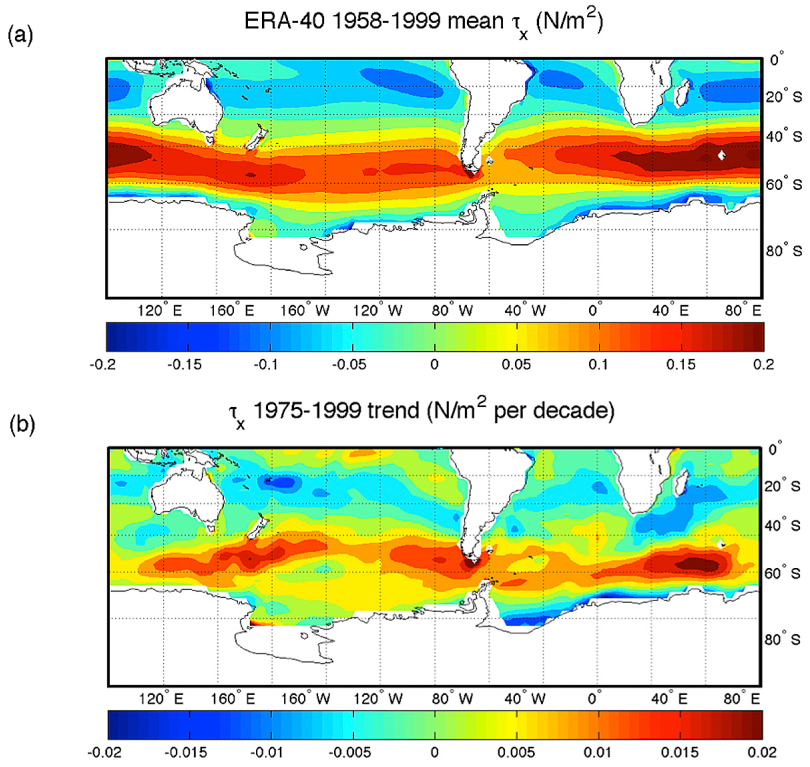

Figure 2. East-west component of surface wind stress based on ERA-40 re-analysis [*Uppala et al.*, 2005]. (a) Climatology (N m^{-2}) and (b) 1975–1999 linear trend (N m^{-2} per decade).

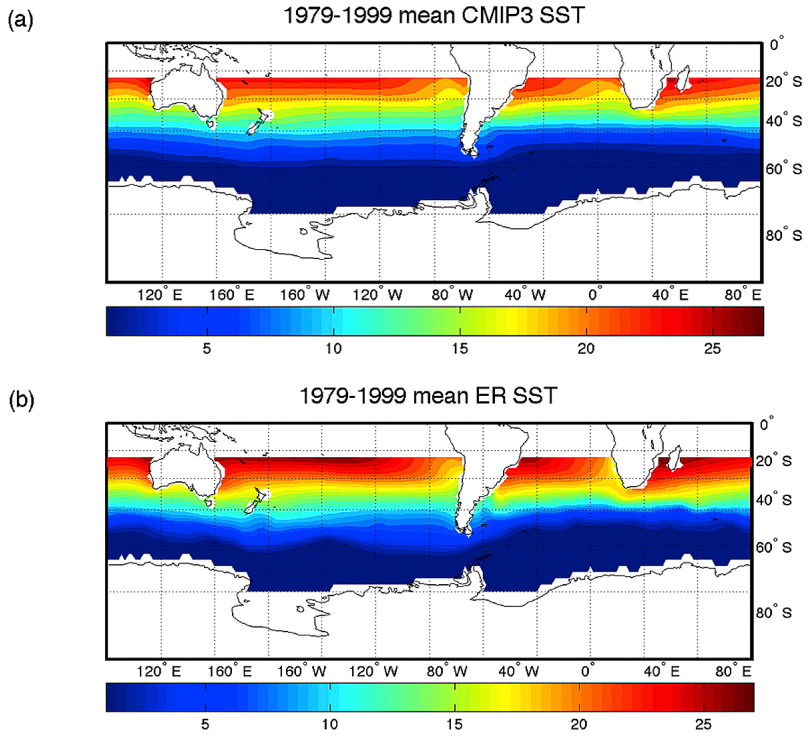

Figure 3. Climatology of sea-surface temperature (°C) based on 1979–1999 data. (a) Multimodel ensemble mean of CMIP3 20th century climate simulations [*Meehl et al.*, 2007]; the members of the ensemble used here are described by *Kravtsov and Spannagle* [2008]. (b) Observed climatology [*Smith et al.*, 2008].

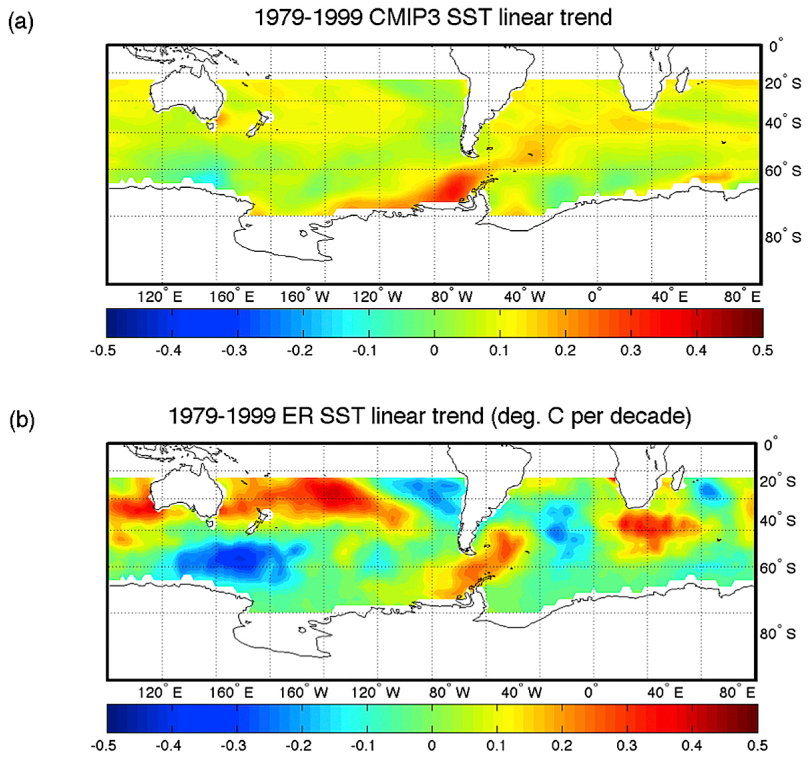

Figure 4. Linear trends of sea-surface temperature (°C per decade) based on 1979–1999 data. (a) Multi-model ensemble mean of CMIP3 20th century climate simulations [*Meehl et al.*, 2007]; the members of the ensemble used here are described by *Kravtsov and Spannagle* [2008]. (b) Observed trends [*Smith et al.*, 2008].

underestimation of the late 20th century surface-wind intensification by the CMIP3 ensemble, and demonstrate strong (and expected) sensitivity of the SST values to the local winds and associated Ekman transport and latent/sensible heat fluxes. The similarity between the observed and simulated zonally averaged SST trends in the presence of the leading-order differences in the wind stress forcing raises a number of questions. In particular, were the CMIP3 models to reproduce, in the 20th century runs, stronger wind stress changes more consistent with observations, would they then simulate unrealistic surface climate response over the ACC? What processes, missing in these simulations, will then need to be included to correct for this bias?

[14] A variety of modeling and observational studies emphasized the importance of mesoscale eddies in the subsurface response of the Southern Ocean to the external forcing (see section 1); clearly, the associated dynamics are not fully represented in the coarse-resolution CMIP3 models. What is the role of the mesoscale oceanic eddies in the *surface* climate response over the ACC region?

3. Results From Idealized Model Simulations

3.1. Eddy-Resolving Quasi-Geostrophic Circulation Model (Q-GCM)

[15] We studied potential effects of mesoscale turbulence on the forced SST evolution in the ACC region by analyzing simulations of the three-layer eddy-resolving quasi-geostrophic general circulation model (Q-GCM, version 1.3.1 [*Hogg et al.*, 2003a, 2003b]) in the ocean-interior–mixed-layer configuration used by *Hogg et al.* [2008]. This configuration includes the Southern Ocean's topography and a constant-depth mixed layer in which time-dependent SSTs can deviate from the radiative equilibrium profile due to air-sea heat exchange, as well as to the heat transports associated with geostrophic and Ekman advection (see *Hogg et al.* [2008, section 2] for further details of the model). While this model is dynamically idealized in the sense that it does not resolve explicitly the thermodynamics of the ACC region, it is ideally suited for simulation of the ocean circulation's perturbations about the mean state, including those due to nonlinear processes and eddies; see an example of Q-GCM simulated eddy field in Figure 5 (top).

[16] The Q-GCM was forced by the zonally symmetric sinusoidal wind stress, which approximately represented the observed wind stress distribution shown in Figure 2a. We performed a 50-yr-long control simulation with the constant wind stress and used the model states from years 20, 30, 40 and 50 of this simulation to initialize the perturbation experiments forced by variable wind stress. In particular, each of these perturbation experiments was forced by linearly increasing the magnitude of the initial wind stress pattern at a specified rate; we used three different rates of about 3, 7, and 10% per decade (within the range of the observed rates, which can be inferred from Figure 2b). We then computed the linear trends of ensemble-mean SST response for each value of the wind stress trend.

[17] The results are summarized in Figure 5 (bottom), which shows the dependence of the south-north SST difference trend on the rate of change of the wind stress

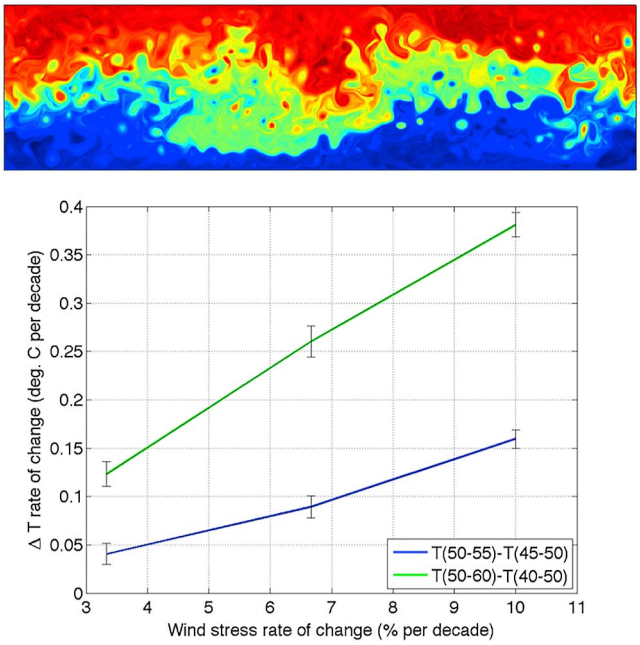

Figure 5. Q-GCM results. (top) Snapshot of the mid-depth potential vorticity from a Q-GCM simulation. (bottom) Trend in the south-north temperature difference as a function of the magnitude of wind stress trend; error bars are determined based on 4-member ensemble of model simulations for each of the three wind stress trend values considered.

forcing. The temperature difference was computed for SSTs averaged within 55°–50°S and 50°–45°S belts (blue line), as well as within 60°–50°S and 50°–40°S belts (green line); this quantity is negative since the temperature increases toward the equator. In all cases, the magnitude of the south-north SST contrast is decreasing, as indicated by a positive trend in Figure 5 (bottom). This decrease is consistent with the case study by *Hogg et al.* [2008]; in the present paper, we extended the Hogg et al.'s results to a wider range of wind stress forcing changes to provide a quantitative estimate of the large-scale SST-gradient anomalies arising from the wind stress induced enhancement of eddy mixing (see below). Note that the vertical heat fluxes through the base of the mixed layer are held steady in our Q-GCM experiments [see *Hogg et al.*, 2008] and, therefore, cannot change the SST contrast. In the absence of eddies, the diagnosed Ekman transports induce basin-wide cooling most pronounced in the middle of the channel (not shown); the associated SST trends are, however, significantly smaller than those associated with eddies. In other words, the eddy-induced south-north SST mixing overwhelms the non-uniform basin-wide SST cooling associated with the weakly intensifying northward Ekman heat transport. For the wind stress increase of about 7% per decade—in the middle of the observed wind stress change range—the simulated 60°–50°S SST warming rate is of about 0.1°C per decade, which is on the same order of magnitude as the CMIP3 simulated radiatively forced SST trends over the ACC (Figure 1a).

[18] The nature of the SST response in the ACC region is linked to this region's being in the so-called eddy saturated state [*Hogg et al.*, 2008], in which increased momentum input transmits directly to the eddy field—that is, makes currents more variable—rather than increasing long-term time-mean currents [*Meredith et al.*, 2004; *Hallberg and Gnanadesikan*, 2006]. Increased mesoscale turbulence mixes warmer water in the northern part of the Southern Ocean with colder water in the south, thus resulting in the reduction of the south-north SST contrast.

[19] Note that the Q-GCM is a perturbation model in which the interior stratification is fixed at zero order and the layer-depth anomalies do not induce vertical heat fluxes at the base of the mixed layer. The effect of eddies on SST in the Q-GCM mixed layer evident in Figure 5 is thus principally different from the eddy-induced changes in subsurface stratification. The essence of the latter subsurface effect is the net tendency of the intensified eddy fluxes to flatten isopycnals across the ACC, which, while resulting in warmer subsurface temperatures south of the ACC and cooler subsurface temperature north of the ACC, has a very weak—and, in fact, oppositely signed—surface manifestation [see *Fyfe et al.*, 2007, Figure 5]. These considerations are further elaborated upon in section 3.2.

3.2. Hybrid Coupled General Circulation Model (H-GCM)

[20] While the Q-GCM provides estimates of the eddy-induced SST trends in the ACC region, it cannot accurately account for many other factors that may affect the SST evolution. In order to address this issue, we deployed a hybrid coupled general circulation model (H-GCM), whose oceanic component is similar to CMIP3 models in several aspects of its design. Model settings and simulated ocean state are very similar to those of *Kamenkovich* [2005]; only a brief description is given here. The model is set up in a global domain extending from 78°S to 84°N using coarse 2° × 2° horizontal resolution and 25 vertical levels with the spacing between the levels increasing toward the bottom. The model bathymetry is derived from the Scripps Topography [*Gates and Nelson*, 1975].

[21] Heat and salt transports by the mesoscale eddies are parameterized using the Gent-McWilliams (GM) scheme [*Gent and McWilliams*, 1990] with constant isopycnal diffusivity of 500 $m^2\ s^{-1}$. Following the standard GM formulation, when the isopycnal slope exceeds a fairly large value of 1/100, the horizontal diffusivity of 500 $m^2\ s^{-1}$ is used and the isopycnal diffusivity is tapered to zero. The K-profile (KPP) parameterization scheme [*Large et al.*, 1994] is used to represent turbulent mixing within a boundary layer.

[22] In addition to these standard options, we also included the surface-intensified horizontal diffusion with the nominal diffusivity of about 1500 $m^2\ s^{-1}$ in the upper 25 m of the ocean (and exponentially decaying to nearly zero below 100-m depth)—$K_H(z) = 5000\ m^2\ s^{-1} \times \exp(-z/10\ m)$ (z is depth in meters)—to reflect the eddy-induced surface mixing. The idea behind this highly idealized representation of the near-surface eddy mixing is to have the most transparent and easily controllable method of varying the intensity of the surface eddy mixing and demonstrating its importance for the SST response. Note that the introduction of lateral mixing in the mixed layer by itself is not new and is a standard part of the GM scheme.

[23] The atmosphere was represented by an energy-balance boundary layer model [*Seager et al.*, 1995]. This model computes air temperature and humidity and returns

air-sea fluxes using the ocean-model simulated SST; other key atmospheric variables, such as vector wind, cloud cover, solar irradiance and air temperature/humidity over land, are prescribed from observational data sets. During the coupling, the oceanic component is forced by the heat fluxes calculated by the atmospheric model, but the wind stress and freshwater fluxes are prescribed, hence the name "hybrid" coupled model. The prescribed wind fields, as well as air temperature and humidity over land were derived from the ECMWF re-analysis. Cloud cover and solar radiation were taken from the International Satellite Cloud Climatology Project, and freshwater fluxes—from the data sets of *Jiang et al.* [1999], which include river runoff data. The annual cycle was retained in all prescribed fields. To avoid a drift in surface salinity toward unrealistic values, it was weakly nudged toward the Levitus climatology using the restoring timescale of 180 days.

[24] The H-GCM also incorporated a thermodynamic sea-ice model [*Visbeck et al.*, 1998]. To keep the amount of sea ice in the model close to observations, we employed the "ice correction," by introducing in the ice-covered areas an anomalous heat flux out of the ocean, which was proportional to the difference between the observed and model-simulated ice cover. The observed ice-cover values for years 1979–2001 were taken from the National Snow and Ice Data Center data set.

[25] After the 1,000-year spin-up using the forcing based on 1990–1995 climatology (prior to a coupled spin-up, the oceanic component has been spun-up for 5,400 years in a stand-alone mode), the H-GCM "global warming" (GW) control run was forced by a linearly increasing solar constant, at the rate of 3% per 70 yr, and fixed climatological winds and clouds, to mimic, in an idealized fashion, projected changes in the net radiative forcing. The linear SST trend from this simulation (Figure 6a) is similar, in both the magnitude and overall latitudinal pattern, to the 1979–1999 trend of CMIP3 ensemble-mean SSTs (see Figure 4a), except for the large positive SST trends just upstream of the Drake Passage simulated by the CMIP3 models but absent in the H-GCM simulation. The latter discrepancy occurs in the region covered by the sea ice during a part of the year. It is largely due to the strong relaxation of the sea-ice cover in the model to its observed climatological distribution ("ice correction" above). This bias is unlikely to affect our main conclusions that pertain to the surface climate variability in the ice-free regions of the model.

[26] Next, we conducted two 25-yr-long sensitivity experiments. In the experiment WIND, we complemented the forcing used in GW experiment by adding the observed 1979–1999 linear trends to the climatological distributions of wind stress, wind speed and velocities south of 30°S. The resulting SST trends displayed in Figure 6b show a mixture of localized patches characterized by strong surface cooling and warming (compare with observations shown in Figure 4b). These tendencies are due to a combination of geographically varying trends in Ekman transport and surface heat flux in response to intensifying winds (compare with *Sallée et al.* [2010]). The zonally averaged trends of both ERSST observed (Figure 1a) and H-GCM simulated SSTs (not shown) are both substantially smaller than their respective local trends due to cancellation between warming and cooling regions. The important difference, however, is the substantial average *cooling* in the experiment WIND, at about the same rate (of about 0.05°C per decade) but in contrast to the overall observed *warming* in the ACC region (see Figure 1a).

[27] In the other sensitivity experiment—EDDIES—we did not include either GW or Wind-forcing. Instead, we approximated the Q-GCM predicted ACC eddy intensification in response to increasing wind stress by the 10% per decade increase in the GM coefficient, as in the work of *Fyfe et al.* [2007], but also by the same-rate increase in the surface horizontal diffusivity south of 30°S. The resulting SSTs south of 30°S exhibit warming (Figure 6c) and corroborate the Q-GCM based estimates of the surface ACC warming rate due to eddies of about 0.1°C per decade. This estimate of the H-GCM simulated SST trend is, of course, sensitive to the surface horizontal mixing used here, in particular on both the value of the surface diffusivity and its increase with winds. Our key point is, however, that without increasing, along with the GM diffusivity in the ocean interior, the mixed-layer lateral diffusivity, the ACC surface warming simulated by H-GCM and displayed in Figure 6c cannot be captured. Indeed, an additional supporting simulation with the GM mixing increase only (not shown) produces an order-of-magnitude weaker SST trends than in EDDIES, consistent with the estimates of *Fyfe et al.* [2007, Figure 5]. Therefore, while the subsurface stratification is sensitive to the increase in the GM mixing, these effects have a weak surface signature.

[28] We must note that the contributions of various dynamical factors that affect the SST trends in the H-GCM turn out to be linear in the sense that the experiments which combine GW, WINDS and EDDIES forcing (not shown) produce the trends that are essentially identical to the sum of the trends due to individual forcing factors in Figure 6, and the zonally averaged SST response to the increasing wind over the ACC consistent with the linear trends in Figure 1a. In particular, in the experiment with the GW, WIND and EDDIES forcing, the effect of basin-mean SST cooling due to intensifying winds is substantially offset by the opposing effect of increasing eddy mixing.

[29] Finally, we take steps toward further disentangling the H-GCM simulated SST response in the ACC region to the structure of wind perturbations. In particular, observations show that not only has the zonal wind stress over ACC region increased in strength over recent decades, but that the location of the maximum wind stress has moved by about 3° to the south. Following *Gent and Danabasoglu*'s [2011] study, we perform two additional experiments in which we add, to our GW forced runs, different idealized perturbations in the zonal wind stress field only. In these experiments, in contrast to the H-GCM experiments described thus far, the vector winds which advect the atmospheric fields in the boundary layer, as well as wind speeds in the bulk formulas for the air-sea fluxes, remained unperturbed. In the first experiment (GW + WIND SHIFT + WIND AMPL.), we introduced the zonal wind stress perturbation characterized by the linear in time shift of the zonal wind stress maximum southward by 3° over 25 years accompanied by the linear in time amplification of the zonal wind stress south of 35°S by 25% over 25 years; the latter amplification coefficient was linearly decreased to unity between 35°S and 20°S. The SST trends arising from this

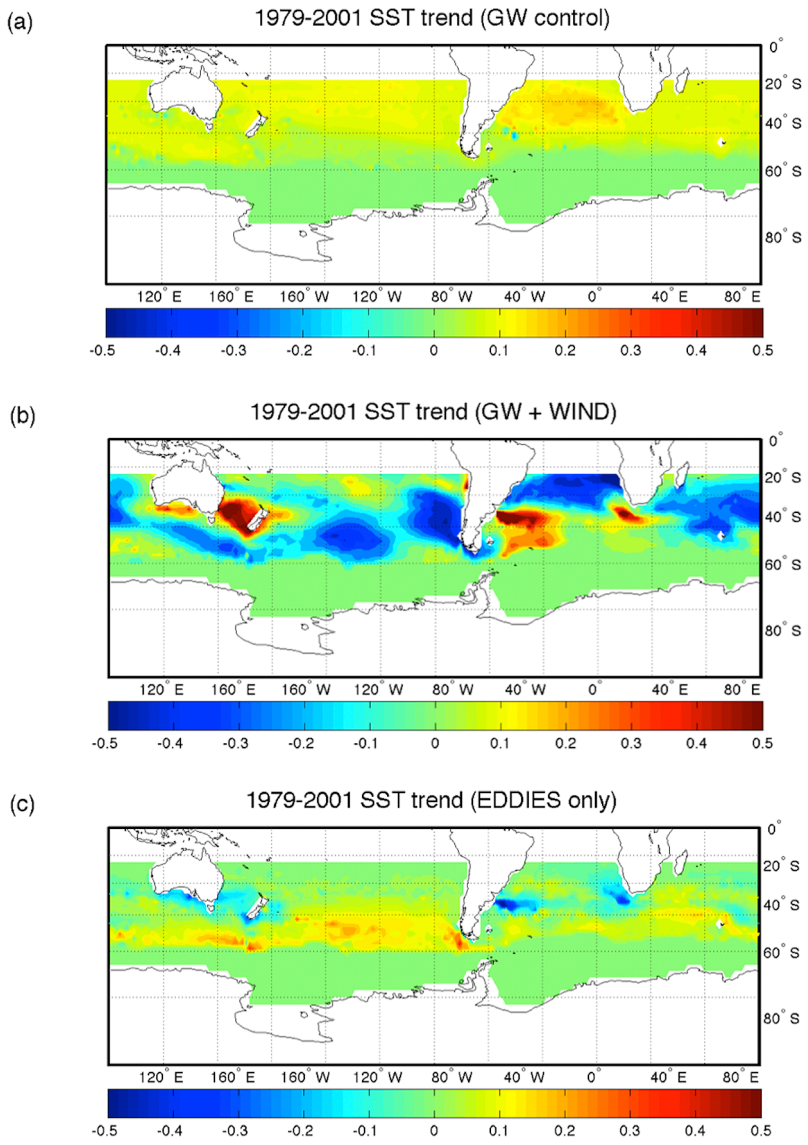

Figure 6. H-GCM results. SST trends (°C per decade) simulated in (a) standard global warming experiment (GW), (b) WIND experiment forced as in the GW experiment plus by increasing surface winds, and (c) EDDIES experiment with climatological forcing and linearly increasing eddy diffusivities. SST anomalies in the sea-ice areas south of 60° S (not shown) are set to zero. See text for details.

experiment are shown in Figure 7a and are qualitatively similar to those derived from our WINDS experiment (Figure 6b). In the second zonal wind stress perturbation experiment (GW+WIND SHIFT, Figure 7b), we only introduced the zonal wind stress shift and skipped the zonal wind stress amplification. The difference between SST trends from these two zonal wind stress perturbation experiments (Figure 7c) isolates the consequences of the zonal-wind stress intensification, which turn out to have an SST anomaly with a similar pattern, but of the opposite sign, relative to the SST anomaly arising from eddy-induced surface mixing shown in Figure 6c. These results allow us to conclude that the main surface effect of ocean eddies (simulated here by means of increasing GM and horizontal surface diffusivity) in the northern ACC region is to partly compensate SST trends due to wind stress *amplification*. This effect is achieved via the enhanced eddy mixing counteracting Ekman-transport dominated cooling in the mixed layer.

4. Conclusions and Discussion

[30] The CMIP3 model ensemble underestimates the observed intensification of westerlies over the Southern Ocean in the late 20th century (Figure 1b). This results in a weaker geographical variation of simulated SST trends compared to the observed ones (Figure 4), albeit fairly similar zonally averaged SST trends over the ACC (Figure 1a). Were the CMIP3 models to produce a stronger—and more realistic—surface-wind intensification, they would have likely exhibited surface cooling over the ACC due to a combined effect of increased surface heat loss and Ekman

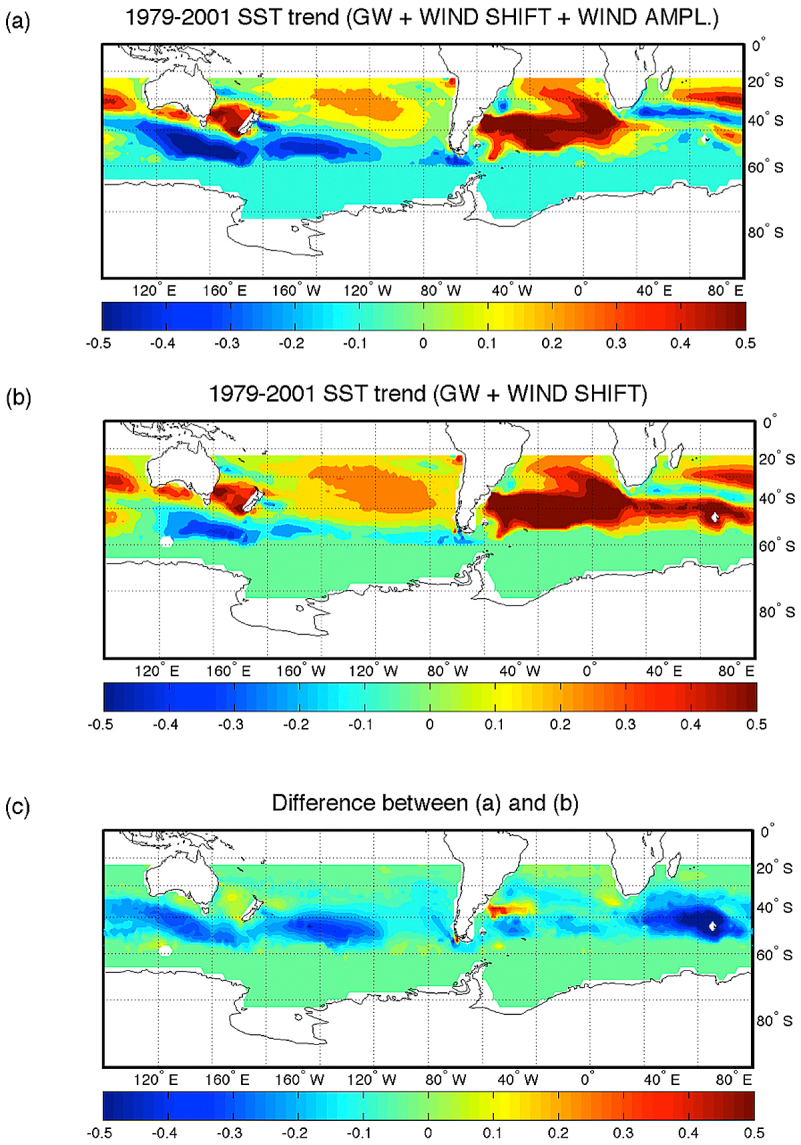

Figure 7. Effects of wind stress changes on SST trends (°C per decade) over the Southern Ocean: (a) the GW experiment in which the zonal wind stress increases with time and shifts to the south, (b) as in Figure 7a but with wind stress shift only; (c) the difference in SST trends derived from experiments in Figures 7a and 7b, which isolates the effect of wind intensification.

transports, as shown by our simulation using an idealized hybrid coupled model (Figures 6b and 7). An important compensation mechanism involves enhanced eddy mixing of SSTs in response to intensified winds (Figure 5); this effect needs to be represented, in CMIP3-type coarse-resolution models, via surface-intensified lateral mixing. Subsurface adiabatic mixing alone is not capable of capturing this important process ocean. In order to illustrate the importance of surface eddies in the present study, the simplest form of such an additional eddy parameterization— a horizontal surface diffusivity linearly increasing with the winds—is shown to effectively compensate for the basin-mean cooling effect of intensifying winds in the ACC region (compare Figures 6c and 7c).

[31] The effect of eddy compensation on the climate change over the Southern Ocean has recently received much attention and sparked the discussions from a variety of perspectives, including analyses based on observations [*Meredith and Hogg*, 2006; *Böning et al.*, 2008], simulations using idealized [*Hogg et al.*, 2008] and comprehensive coarse-resolution [*Fyfe et al.*, 2007], as well as eddy-resolving ocean or eddy-permitting climate models [*Hallberg and Gnanadesikan*, 2006; *Screen et al.*, 2009; *Shaffrey et al.*, 2009; *Farneti and Delworth*, 2010; *Farneti et al.*, 2010; *Spence et al.*, 2010]. The latter studies have clearly shown that the response of the southward eddy heat transport in the Southern Ocean to changes in external forcing, achieved in an eddy-permitting climate model, cannot be fully captured by a coarse-resolution model in which eddy effects are parameterized using schemes with either the constant GM coefficient or with the GM coefficient whose value is not allowed to exceed a low threshold.

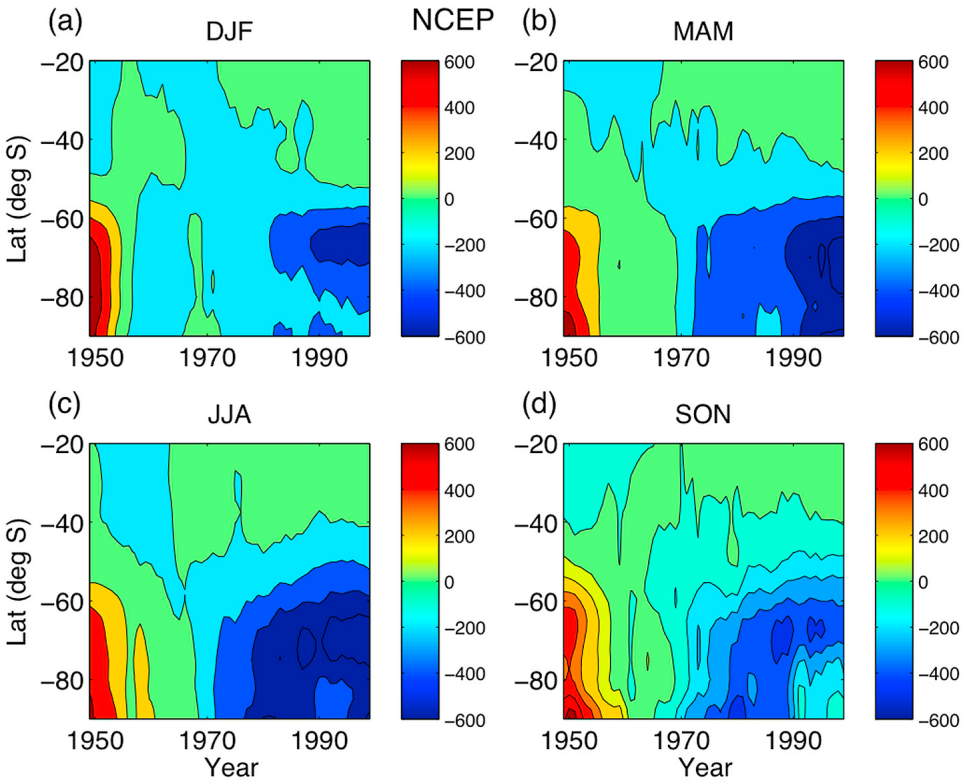

Figure A1. Time-latitude diagram of the observed seasonal zonal-mean sea level pressure (SLP) anomalies (Pa) computed relative to the 1951–1980 time-mean SLP, based on NCEP/NCAR re-analysis product [*Kalnay et al.*, 1996]. (a) DJF, (b) MAM, (c) JJA, and (d) SON seasons. The time series shown have been smoothed using 10-yr boxcar running mean filter.

Fyfe et al. [2007] introduced, with some success, an ad hoc perturbation of the GM coefficient to parameterize this crucial eddy effect. However, the surface signature of SST trends due to the anomalous eddy-induced residual-mean circulation they have modeled was very small—the result that our H-GCM simulation with increasing GM coefficient and fixed lateral heat diffusivity at the surface replicates. The wind-induced subsurface intensification of eddy activity is apparently incapable of producing a significant SST response.

[32] On the other hand, when the mixing effect of mesoscale eddies at the surface are taken into account, the SST response to increased eddy activity is altered substantially and becomes quantitatively important. In particular, our study demonstrates that the eddy induced SST mixing can effectively counteract the basin-mean surface cooling due to air-sea heat exchange and Ekman transport anomalies associated with intensified winds. This result was obtained here using a trivial and perhaps over-simplified model for surface eddy intensification involving additional surface horizontal diffusivity linearly tied to the surface-wind intensity. This scheme was used for illustrative purposes only. While it captures a qualitative picture of the eddy response to the winds in the eddy-saturated regime the ACC is believed to be operating in, more dynamically justified parameterizations of these processes are needed in climate-change studies that use coarse resolution ocean models.

[33] A number of such parameterizations have recently been discussed in the literature [*Farneti and Gent*, 2011; *Hofmann and Morales-Maqueda*, 2011; *Gent and Danabasoglu*, 2011]. In these papers, the authors argue that the appropriate response of the Southern Ocean to the intensifying winds can be achieved in the coarse-resolution climate models in which the eddy parameterization involves a non-constant, in space and time, GM coefficient tied to ocean variables. Furthermore, for the correct ocean response, it is essential not to restrict too severely the value of this variable GM coefficient (compare *Farneti et al.* [2010] with *Farneti and Gent* [2011] and *Hofmann and Morales-Maqueda* [2011]). Finally, as corroborated by our results, the variable GM coefficients in the ocean interior have to be matched with the horizontal eddy diffusion in the ocean mixed layer to capture the eddy-induced surface response to variable forcing factors, as is done, for example, in the work of *Gent and Danabasoglu* [2011]. Several advanced, physically based parameterization schemes for mixed-layer eddies have been developed recently [see, e.g., *Fox-Kemper and Ferrari*, 2008; *Fox-Kemper et al.*, 2011].

[34] These ideas have important implications for predicting the Southern Hemisphere future climate change [*Shindell and Schmidt*, 2004; *Arblaster et al.*, 2011]. As the winds continue to respond to variable radiative and natural forcings, the combined direct effect of ensuing changes in surface heat flux and Ekman transports and indirect effect of modified eddy mixing will affect the sign and magnitude of

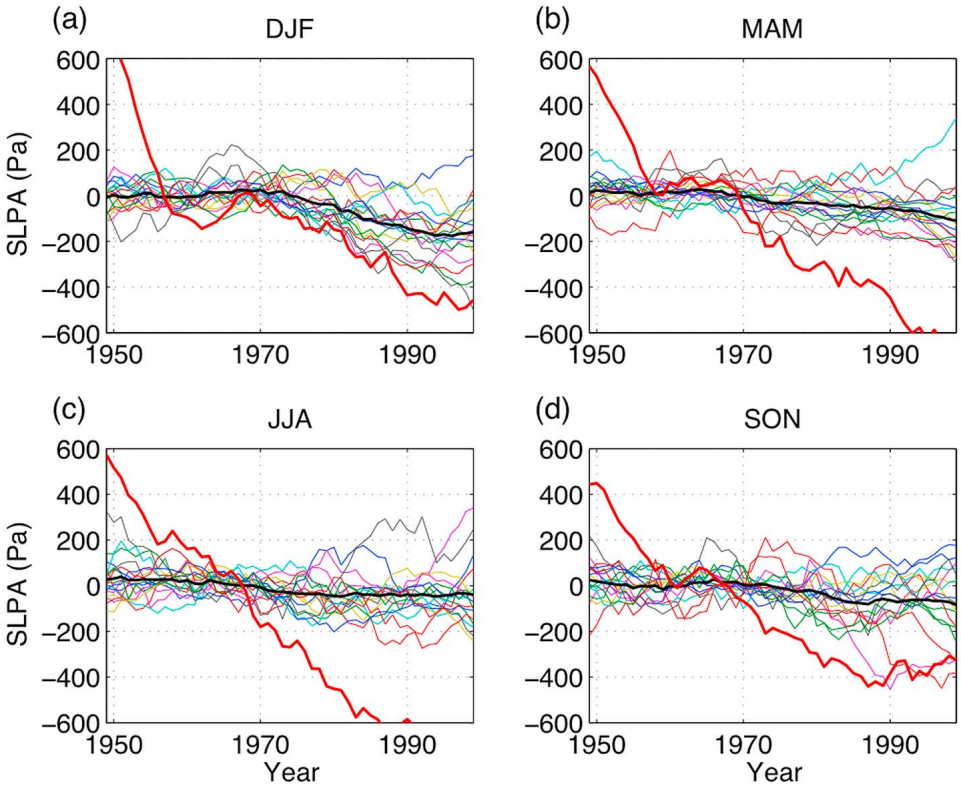

Figure A2. Observed and simulated seasonal sea level pressure (SLP) anomalies at 70°S (relative to 1951–1980 base period). (a) DJF, (b) MAM, (c) JJA, and (d) SON. Thick red line, NCEP-NCAR reanalysis [*Kalnay et al.*, 1996]; thin colored lines, individual CMIP3 models' ensemble means; thick black line, multimodel ensemble average. The members of the CMIP3 ensemble used here are described by *Kravtsov and Spannagle* [2008]. The observed time series have been smoothed using 10-yr boxcar running-mean filter.

SST anomalies in the ACC region, with further possible ocean-atmosphere feedbacks on the strength of the atmospheric jet stream [*Marshall and Connolley*, 2006; *Cai and Cowan*, 2007; *Hogg et al.*, 2009]. These processes have to be accounted for in obtaining accurate estimates of global climate sensitivities. Complexity and importance of the eddy dynamics in the Southern Ocean may require the climate models to have eddy-resolving ocean components for correctly simulating this region's response to variable external forcing.

Appendix A: Alternative Observational Data Sets and Seasonal Dependence of the Results

[35] In this section, we look at the observed sea level pressure (SLP) trends using the NCEP/NCAR re-analysis product [*Kalnay et al.*, 1996] and SST trends computed for GISS data set [*Hansen et al.*, 1999, 2001]. The GISS data set SST measurements are based on ship data prior to 1981 (HadlSST1 data set [*Rayner*, 2000; *Rayner et al.*, 2003]), and include satellite observations after that time [*Reynolds and Smith*, 1994; *Reynolds et al.*, 2002; *Smith and Reynolds*, 2004]. We also use here a slightly different way—compared to that in the main text—of visualizing secular variability, namely, instead of computing linear trends, we apply a 10-yr boxcar running-mean filter to the observed data. The SST data set and data pre-processing are identical to those of *Kravtsov and Spannagle* [2008]. All of the results are shown for each of the four seasons: DJF, MAM, JJA, and SON.

[36] The time dependence of zonal-mean SLP anomalies is visualized in Figure A1. The main feature of the observed SLP evolution for all seasons is a largely monotonic decrease south of 50° S, with a much smaller opposite trend to the north of this latitude. Motivated by this latitudinal pattern of zonally averaged SLP trends, we used the time series of SLP anomaly at 70°S in lieu of the Southern Hemisphere Annular Mode (SAM) index; negative values of this index correspond to stronger polar vortex and increased winds over the Southern Ocean. The observed and simulated indices are displayed in Figure A2, and show large differences between the actual and CMIP3 modeled SLP trends throughout the year. The SAM trends deduced from NCEP data are stronger than those based on ERA-40 data, and are likely to be overestimated [*Thompson and Solomon*, 2002; *Marshall*, 2003]. Still, the considerable differences between the observations and CMIP3 models are detected in both re-analysis products.

[37] Finally, Figure A3 reiterates the main premise of our work: Despite underestimating wind intensification over the ACC, the CMIP3 models capture zonal-mean SST trends over the Southern Ocean in the late 20th century amazingly well. We argue that this is partly due to CMIP3 models

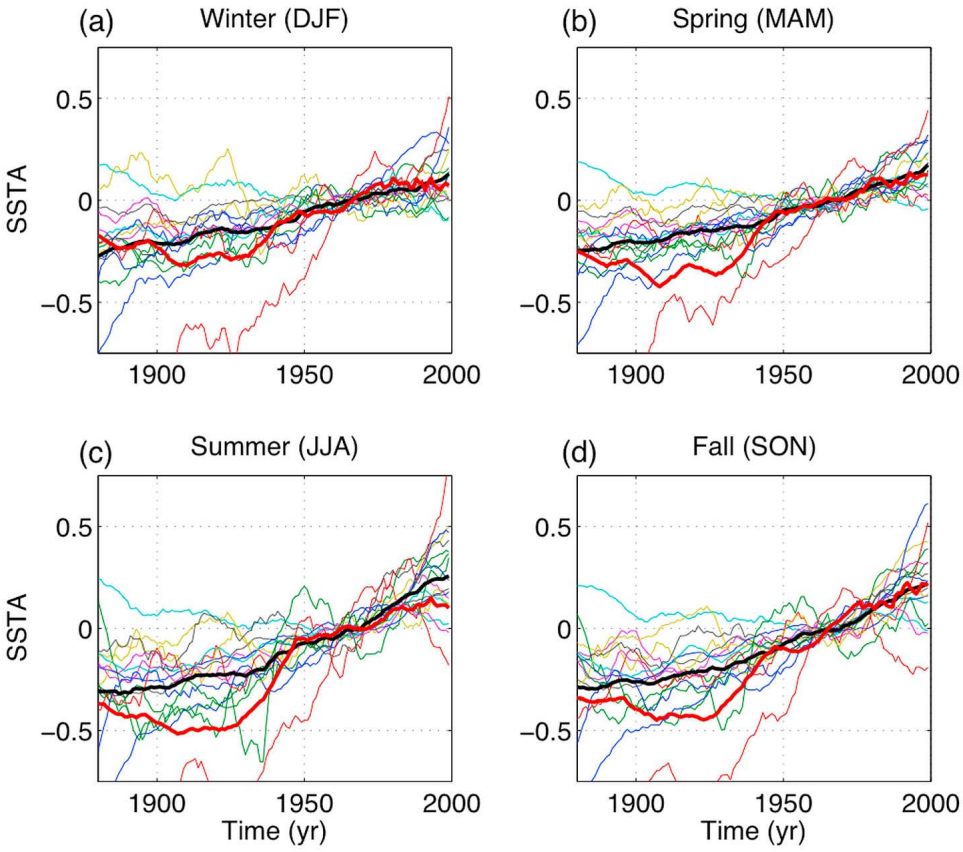

Figure A3. Observed and simulated seasonal sea-surface temperature (SST) anomalies (relative to 1951–1980 base period) area-averaged over 60°–50°S belt: (a) DJF, (b) MAM, (c) JJA, and (d) SON. Thick red line, SST based on GISS data set [*Hansen et al.*, 1999, 2001] (see text for further details); thin colored lines, individual CMIP3 models' ensemble means; thick black line, multimodel ensemble average. The members of the CMIP3 ensemble used here are described by *Kravtsov and Spannagle* [2008]. The observed time series have been smoothed using 10-yr boxcar running-mean filter.

making two large opposing errors which balance each other (see the main text).

[38] **Acknowledgments.** We are grateful to William Dewar, Till Kuhlbrodt, Peter Gent, Frank Bryan and three anonymous reviewers for useful comments on aspects of this work. This research was supported by the Office of Science (BER), U.S. Department of Energy (DOE) grant DE-FG02-07ER64428, as well as by 2009 UWM RGI grant (S.K. and J.M.P.), NSF grant OCE-0749723 (I.K.), and ARC Discovery Project DP0877824 (A.H.). We acknowledge modeling groups, PCMDI, and WCRP's WGCM for their roles in making CMIP3 set available, and DOE for this data set's support. ECMWF ERA-40 data used in this have been obtained from the ECMWF data server.

References

Arblaster, J. M., and G. A. Meehl (2006), Contributions of external forcings to Southern Annular Mode trends, *J. Clim.*, *19*, 2896–2905, doi:10.1175/JCLI3774.1.

Arblaster, J. M., G. A. Meehl, and D. J. Karoly (2011), Future climate change in the Southern Hemisphere: Competing effects of ozone and greenhouse gases, *Geophys. Res. Lett.*, *38*, L02701, doi:10.1029/2010GL045384.

Böning, C. W., A. Dispert, M. Visbeck, S. R. Rintoul, and F. U. Schwarzkopf (2008), The response of the Antarctic Circumpolar Current to recent climate change, *Nat. Geosci.*, *1*, 864–869, doi:10.1038/ngeo362.

Cai, W., and T. Cowan (2007), Impacts of increasing anthropogenic aerosols on the atmospheric circulation trends of the Southern Hemisphere: An air-sea positive feedback, *Geophys. Res. Lett.*, *34*, L23709, doi:10.1029/2007GL031706.

Cai, W., G. Shi, T. Cowan, D. Bi, and J. Ribbe (2005), The response of the Southern Annular Mode, the East Australian Current, and the southern mid-latitude ocean circulation to global warming, *Geophys. Res. Lett.*, *32*, L23706, doi:10.1029/2005GL024701.

Cai, W., D. Bi, J. Church, T. Cowan, M. Dix, and L. Rotstayn (2006), Pan-oceanic response to increasing anthropogenic aerosols: Impacts on the Southern Hemisphere oceanic circulation, *Geophys. Res. Lett.*, *33*, L21707, doi:10.1029/2006GL027513.

Cai, W., T. Cowan, J. M. Arblaster, and S. Wijffels (2010a), On potential causes for an under-estimated global ocean heat content trend in CMIP3 models, *Geophys. Res. Lett.*, *37*, L17709, doi:10.1029/2010GL044399.

Cai, W., T. Cowan, S. Wijffels, and S. Godfrey (2010b), Simulations of processes associated with the fast warming rate of the southern midlatitude ocean, *J. Clim.*, *23*, 197–206, doi:10.1175/2009JCLI3081.1.

Farneti, R., and T. L. Delworth (2010), The role of mesoscale eddies in the remote oceanic response to altered Southern Hemisphere winds, *J. Phys. Oceanogr.*, *40*, 2348–2354, doi:10.1175/2010JPO4480.1.

Farneti, R., and P. R. Gent (2011), The effects of the eddy-induced advection coefficient in a coarse-resolution coupled climate model, *Ocean Modell.*, *39*, 135–145, doi:10.1016/j.ocemod.2011.02.005.

Farneti, R., T. L. Delworth, A. J. Rosati, S. M. Griffies, and F. Zeng (2010), The role of mesoscale eddies in the rectification of the Southern Ocean response to climate change, *J. Phys. Oceanogr.*, *40*, 1539–1557, doi:10.1175/2010JPO4353.1.

Fox-Kemper, B., and R. Ferrari (2008), Parameterization of mixed layer eddies. Part II: Prognosis and impact, *J. Phys. Oceanogr.*, *38*, 1166–1179, doi:10.1175/2007JPO3788.1.

Fox-Kemper, B., G. Danabasoglu, R. Ferrari, S. M. Griffies, R. W. Hallberg, M. M. Holland, M. E. Maltrud, S. Peacock, and B. L. Samuels (2011), Parameterization of mixed layer eddies. III: Implementation and impact

in global ocean climate simulations, *Ocean Modell.*, *39*, 61–78, doi:10.1016/j.ocemod.2010.09.002.
Fyfe, J. C. (2006), Southern Ocean warming due to human influence, *Geophys. Res. Lett.*, *33*, L19701, doi:10.1029/2006GL027247.
Fyfe, J. C., and O. A. Saenko (2006), Simulated changes in extratropical Southern Hemisphere winds and currents, *Geophys. Res. Lett.*, *33*, L06701, doi:10.1029/2005GL025332.
Fyfe, J. C., O. A. Saenko, K. Zickfield, M. Eby, and A. J. Weaver (2007), The role of poleward-intensifying winds on Southern Ocean warming, *J. Clim.*, *20*, 5391–5400, doi:10.1175/2007JCLI1764.1.
Gates, W. L., and A. B. Nelson (1975), A new (revised) tabulation of the Scripps Topography on a 1° global grid, Part 2: Ocean depths, *Rep. R-1277-1-ARPA*, 132 pp., RAND Corp., Santa Monica, Calif.
Gent, P. R., and G. Danabasoglu (2011), Response to increasing Southern Hemisphere winds in CCSM4, *J. Clim.*, doi:10.1175/JCLI-D-10-05011.1, in press.
Gent, P. R., and J. C. McWilliams (1990), Isopycnal mixing in ocean general circulation models, *J. Phys. Oceanogr.*, *20*, 150–155, doi:10.1175/1520-0485(1990)020<0150:IMIOCM>2.0.CO;2.
Gille, S. T. (2002), Warming of the Southern Ocean since the 1950s, *Science*, *295*, 1275–1277, doi:10.1126/science.1065863.
Gille, S. T. (2008), Decadal-scale temperature trends in the Southern Hemisphere ocean, *J. Clim.*, *21*, 4749–4765, doi:10.1175/2008JCLI2131.1.
Gillett, N. P., and D. W. Thompson (2003), Simulation of recent Southern Hemisphere climate change, *Science*, *302*, 273–275, doi:10.1126/science.1087440.
Graham, N. E. (1994), Decadal scale variability in the tropical and North Pacific during the 1970s and 1980s: Observations and model results, *Clim. Dyn.*, *10*, 135–162, doi:10.1007/BF00210626.
Hallberg, R., and A. Gnanadesikan (2006), The role of eddies in determining the structure and response of the wind-driven Southern Hemisphere overturning: Results from the modeling eddies in the Southern Ocean project, *J. Phys. Oceanogr.*, *36*, 2232–2252, doi:10.1175/JPO2980.1.
Hansen, J., R. Ruedy, J. Glascoe, and M. Sato (1999), GISS analysis of surface temperature change, *J. Geophys. Res.*, *104*, 30,997–31,022, doi:10.1029/1999JD900835.
Hansen, J., R. Ruedy, M. Sato, M. Imhoff, W. Lawrence, D. Easterling, T. Peterson, and T. Karl (2001), A closer look at United States and global surface temperature change, *J. Geophys. Res.*, *106*, 23,947–23,963, doi:10.1029/2001JD000354.
Hofmann, M., and M. A. Morales-Maqueda (2011), The response of Southern Ocean eddies to increased midlatitude westerlies: A non-eddy resolving model study, *Geophys. Res. Lett.*, *38*, L03605, doi:10.1029/2010GL045972.
Hogg, A. M., and J. R. Blundell (2006), Interdecadal variability of the Southern Ocean, *J. Phys. Oceanogr.*, *36*, 1626–1645, doi:10.1175/JPO2934.1.
Hogg, A. M., J. R. Blundell, W. K. Dewar, and P. D. Killworth (2003a), Formulation and users' guide for Q-GCM (version 1.0), *Internal Doc. 88*, 44 pp., Natl. Oceanogr. Cent., Southampton, U. K., 25 March.
Hogg, A. M., W. K. Dewar, P. D. Killworth, and J. R. Blundell (2003b), A quasi-geostrophic coupled model (Q-GCM), *Mon. Weather Rev.*, *131*, 2261–2278, doi:10.1175/1520-0493(2003)131<2261:AQCMQ>2.0.CO;2.
Hogg, A. M., M. P. Meredith, J. R. Blundell, and C. Wilson (2008), Eddy heat flux in the Southern Ocean: Response to variable wind forcing, *J. Clim.*, *21*, 608–620, doi:10.1175/2007JCLI1925.1.
Hogg, A. M., W. K. Dewar, P. Berloff, S. Kravtsov, and D. K. Hutchinson (2009), The effects of mesoscale ocean–atmosphere coupling on the large-scale ocean circulation, *J. Clim.*, *22*, 4066–4082, doi:10.1175/2009JCLI2629.1.
Jiang, S., P. H. Stone, and P. Malanotte-Rizzoli (1999), An assessment of the Geophysical Fluid Dynamics Laboratory ocean model with coarse resolution: Annual-mean climatology, *J. Geophys. Res.*, *104*, 25,623–25,645, doi:10.1029/1999JC900095.
Kalnay, E., et al. (1996), The NCEP/NCAR 40-year reanalysis project, *Bull. Am. Meteorol. Soc.*, *77*, 437–471, doi:10.1175/1520-0477(1996)077<0437:TNYRP>2.0.CO;2.
Kamenkovich, I. V. (2005), Role of daily surface forcing in setting the temperature and mixed layer structure of the Southern Ocean, *J. Geophys. Res.*, *110*, C07006, doi:10.1029/2004JC002610.
Kamenkovich, I. V., and E. S. Sarachik (2004), Mechanisms controlling the sensitivity of the Atlantic thermohaline circulation to the parameterization of eddy transports in ocean GCMs, *J. Phys. Oceanogr.*, *34*, 1628–1647, doi:10.1175/1520-0485(2004)034<1628:MCTSOT>2.0.CO;2.
Kravtsov, S., and C. Spannagle (2008), Multidecadal climate variability in observed and modeled surface temperatures, *J. Clim.*, *21*, 1104–1121, doi:10.1175/2007JCLI1874.1.
Kushner, P. J., I. M. Held, and T. L. Delworth (2001), Southern Hemisphere atmospheric circulation response to global warming, *J. Clim.*, *14*, 2238–2249, doi:10.1175/1520-0442(2001)014<0001:SHACRT>2.0.CO;2.
Large, W. G., J. C. McWilliams, and S. C. Doney (1994), Oceanic vertical mixing: A review and a model with nonlocal boundary layer parameterisation, *Rev. Geophys.*, *32*, 363–403, doi:10.1029/94RG01872.
Marshall, G. J. (2003), Trends in the southern annular mode from observations and reanalyses, *J. Clim.*, *16*, 4134–4143, doi:10.1175/1520-0442(2003)016<4134:TITSAM>2.0.CO;2.
Marshall, J., and T. Radko (2003), Residual-mean solutions for the Antarctic Circumpolar Current and its associated overturning circulation, *J. Phys. Oceanogr.*, *33*, 2341–2354, doi:10.1175/1520-0485(2003)033<2341:RSFTAC>2.0.CO;2.
Marshall, G. J., and W. M. Connolley (2006), The effect of changing Southern Hemisphere winter sea surface temperatures on Southern Annular Mode strength, *Geophys. Res. Lett.*, *33*, L17717, doi:10.1029/2006GL026627.
Marshall, G. J., P. A. Stott, J. Turner, W. M. Connolley, J. C. King, and T. A. Lachlan-Cope (2004), Causes of exceptional atmospheric circulation changes in the Southern Hemisphere, *Geophys. Res. Lett.*, *31*, L14205, doi:10.1029/2004GL019952.
Meehl, G. A., et al. (2007), The WCRP CMIP3 multimodel dataset: A new era in climate change research, *Bull. Am. Meteorol. Soc.*, *88*, 1383–1394, doi:10.1175/BAMS-88-9-1383.
Meredith, M. P., and A. M. Hogg (2006), Circumpolar response of Southern Ocean eddy activity to a change in the Southern Annular Mode, *Geophys. Res. Lett.*, *33*, L16608, doi:10.1029/2006GL026499.
Meredith, M. P., P. L. Woodworth, C. W. Hughes, and V. Stepanov (2004), Changes in the ocean transport through Drake Passage during the 1980s and 1990s, forced by changes in the Southern Annular Mode, *Geophys. Res. Lett.*, *31*, L21305, doi:10.1029/2004GL021169.
Miller, R. L., G. A. Schmidt, and D. T. Shindell (2006), Forced annular variations in the 20th century Intergovernmental Panel on Climate Change Fourth Assessment Report models, *J. Geophys. Res.*, *111*, D18101, doi:10.1029/2005JD006323.
Oke, P. R., and M. H. England (2004), Oceanic response to changes in the latitude of the Southern Hemisphere subpolar westerly winds, *J. Clim.*, *17*, 1040–1054, doi:10.1175/1520-0442(2004)017<1040:ORTCIT>2.0.CO;2.
Radko, T., and I. Kamenkovich (2011), Semi-adiabatic model of the deep stratification and meridional overturning, *J. Phys. Oceanogr.*, *41*, 757–780, doi:10.1175/2010JPO4538.1.
Radko, T., and J. Marshall (2006), The Antarctic Circumpolar Current in three dimensions, *J. Phys. Oceanogr.*, *36*, 651–669, doi:10.1175/JPO2893.1.
Rayner, N. (2000), *HadISST1 Sea Ice and Sea Surface Temperature Files*, Hadley Cent., Bracknell, U. K.
Rayner, N. A., D. E. Parker, E. B. Horton, C. K. Folland, L. V. Alexander, D. P. Rowell, E. C. Kent, and A. Kaplan (2003), Global analyses of sea surface temperature, sea ice, and night marine air temperature since the late nineteenth century, *J. Geophys. Res.*, *108*(D14), 4407, doi:10.1029/2002JD002670.
Reynolds, R. W., and T. M. Smith (1994), Improved global sea-surface temperature analysis using optimum interpolation, *J. Clim.*, *7*, 929–948, doi:10.1175/1520-0442(1994)007<0929:IGSSTA>2.0.CO;2.
Reynolds, R. W., et al. (2002), Improved global sea surface temperature analysis, *J. Clim.*, *15*, 1609–1625, doi:10.1175/1520-0442(2002)015<1609:AIISAS>2.0.CO;2.
Rintoul, S. R., C. W. Hughes, and D. Olbers (2001), The Antarctic Circumpolar Current system, in *Ocean Circulation and Climate: Observing and Modelling the Global Ocean*, *Int. Geophys.*, vol. 77, edited by G. Siedler, J. Church, and J. Gould, pp. 271–302, Academic, London, doi:10.1016/S0074-6142(01)80124-8.
Russell, J. L., R. J. Stouffer, and K. W. Dixon (2006), Intercomparison of the Southern Ocean circulations in the IPCC coupled model control simulations, *J. Clim.*, *19*, 4560–4575, doi:10.1175/JCLI3869.1.
Sallée, J. B., K. G. Speer, and S. R. Rintoul (2010), Zonally asymmetric response of the Southern Ocean mixed-layer depth to the Southern Annular Mode, *Nat. Geosci.*, *3*, 273–279, doi:10.1038/ngeo812.
Screen, J. A., N. P. Gillett, D. P. Stevens, G. J. Marshall, and H. K. Roscoe (2009), The role of the eddies in the Southern Ocean temperature response to the southern annular mode, *J. Clim.*, *22*, 806–818, doi:10.1175/2008JCLI2416.1.
Seager, R., M. B. Blumenthal, and Y. Kushnir (1995), An advective atmospheric mixed-layer model for ocean modeling purposes—Global simulation of surface heat fluxes, *J. Clim.*, *8*, 1951–1964, doi:10.1175/1520-0442(1995)008<1951:AAAMLM>2.0.CO;2.

Shaffrey, L. C., et al. (2009), U. K. HiGEM: The new U. K. high-resolution global environment model—Model description and basic evaluation, *J. Clim.*, *22*, 1861–1896, doi:10.1175/2008JCLI2508.1.

Shindell, D. T., and G. A. Schmidt (2004), Southern Hemisphere climate response to ozone changes and greenhouse gas increases, *Geophys. Res. Lett.*, *31*, L18209, doi:10.1029/2004GL020724.

Sloyan, B. M., and I. V. Kamenkovich (2007), Simulation of Subantarctic Mode and Antarctic Intermediate Waters in climate models, *J. Clim.*, *20*, 5061–5080, doi:10.1175/JCLI4295.1.

Smith, T. M., and R. W. Reynolds (2004), Improved extended reconstruction of SST (1854–1997), *J. Clim.*, *17*, 2466–2477, doi:10.1175/1520-0442(2004)017<2466:IEROS>2.0.CO;2.

Smith, T. M., R. W. Reynolds, T. C. Peterson, and J. Lawrimore (2008), Improvements to NOAA's historical merged land–ocean surface temperature analysis, *J. Clim.*, *21*, 2283–2296, doi:10.1175/2007JCLI2100.1.

Spence, P., J. C. Fyfe, A. Montenegro, and A. J. Weaver (2010), Southern Ocean response to strengthening winds in an eddy-permitting global climate model, *J. Clim.*, *23*, 5332–5343, doi:10.1175/2010JCLI3098.1.

Thompson, D. W. J., and S. Solomon (2002), Interpretation of recent Southern Hemisphere climate change, *Science*, *296*, 895–899, doi:10.1126/science.1069270.

Thompson, D. W. J., J. M. Wallace, and G. C. Hegerl (2000), Annular modes in the extratropical circulation. Part II: Trends, *J. Clim.*, *13*, 1018–1036, doi:10.1175/1520-0442(2000)013<1018:AMITEC>2.0.CO;2.

Tsonis, A. A., K. Swanson, and S. Kravtsov (2007), A new dynamical mechanism for major climate shifts, *Geophys. Res. Lett.*, *34*, L13705, doi:10.1029/2007GL030288.

Uppala, S. M., et al. (2005), The ERA-40 re-analysis, *Q. J. R. Meteorol. Soc.*, *131*, 2961–3012, doi:10.1256/qj.04.176.

Visbeck, M., H. Cullen, G. Krahmann, and N. Naik (1998), An ocean model's response to North Atlantic Oscillation-like wind forcing, *Geophys. Res. Lett.*, *25*, 4521–4524, doi:10.1029/1998GL900162.

Wolfe, C. L., and P. Cessi (2010), What sets the strength of the middepth stratification and overturning circulation in eddying ocean models?, *J. Phys. Oceanogr.*, *40*, 1520–1538, doi:10.1175/2010JPO4393.1.

A. M. Hogg, Research School of Earth Sciences, Australian National University, Canberra, ACT 0200, Australia.

I. Kamenkovich, MPO, RSMAS, University of Miami, 4600 Rickenbacker Cswy., Miami, FL 33149-1031, USA.

S. Kravtsov and J. M. Peters, Department of Mathematical Sciences, Atmospheric Sciences Group, University of Wisconsin-Milwaukee, Milwaukee, WI 53201-0413, USA. (kravtsov@uwm.edu)